EurJIC
European Journal of Inorganic Chemistry

Full Papers
doi.org/10.1002/ejic.202100454

Chemistry Europe
European Chemical Societies Publishing

Speeding-up Thermally Activated Delayed Fluorescence in Cu(I) Complexes Using Aminophosphine Ligands

Jéssica Toigo,[a] Giliandro Farias,[a] Cristian A. M. Salla,[b] Luís Gustavo Teixeira Alves Duarte,[c] Adailton J. Bortoluzzi,[a] Teresa Dib Zambon Atvars,[c] Bernardo de Souza,*[a] and Ivan H. Bechtold*[b]

Luminescent copper(I) complexes presenting thermally activated delayed fluorescence (TADF) have drawn attention as emitters for organic light emitting diodes (OLEDs). While the majority of ligands used have nitrogen as donor atoms, in this work, we report the synthesis and characterization of three copper(I) complexes with the diimine ligand 1,10-phenanthroline and aminophosphine-derived ligands containing the piperazine and *N*,*N*′-dimethylethylenediamine to evaluate their effect into the emission properties. The photophysical studies as a function of temperature suggested TADF and phosphorescence emission, supported by detailed density functional theory (DFT) calculations. The use of aminophosphine ligands enhance the TADF decay pathway in comparison with copper complex containing the usual POP ligand. These properties, combined with the appropriate HOMO-LUMO energy levels and thermal stability, make these compounds a promising alternative for application in OLEDs.

Introduction

The development of new emitters has attracted considerable attention in the last years, mainly for applications in OLEDs.[1] In particular, TADF materials came into focus as a cheaper alternative to the traditional heavy-atom-based phosphorescent materials, such as platinum, osmium, or iridium.[2–4] TADF emitters allow for harvesting both generated singlet and triplet excitons in such devices. As a result, 100% internal quantum efficiency can be achieved with shorter lifetimes, improving the efficiency of electroluminescence devices by reducing the triplet-triplet annihilation (TTA) and triplet-polaron quenching (TPA).[5] Thus, low-cost copper(I) complexes are usually efficient TADF emitters, and their versatile photophysical properties can be modulated by introducing ligands such as diimines and diphosphines.[6,7]

The TADF mechanism mainly relies on thermal energy to harvest electrons from the triplet to the singlet state via reverse intersystem crossing (rISC). For copper(I) complexes, the $\Delta E(S_1–T_1)$ can exhibit different values according to spatially distinct HOMO-LUMO distribution.[7–9] For heteroleptic complexes $[Cu(NN)(PP)]^+$, as the HOMO is usually centered at copper-phosphor moiety and the LUMO on the diimine, even small changes at the ligands affect the $\Delta E(S_1–T_1)$ energy gap.[6,9,10] Moreover, the HOMO and LUMO overlap also affects the allowedness of the $S_1 \rightarrow S_0$ transition and the spin-orbit coupling (SOC) matrix elements between the low-lying state, impacting the overall radiative and non-radiative decay pathways.[7,9] Although several studies have been carried out investigating the influence of diimines on these photophysical properties, especially in the emission color modulation,[11] the structure-property relations of phosphines are still to be elucidated.

Phosphine ligands, such as triphenylphosphine (PPh_3),[12] (Oxydi-2,1-phenylene)bis(diphenylphosphine) (POP)[13,14] and (9,9-Dimethyl-9H-xanthene-4,5-diyl)bis(diphenylphosphine) (Xantphos)[15,16] were first introduced to heteroleptic copper(I) complexes in order to improve their electrochemical and stability properties.[6] Chelating phosphines such as POP and Xanthphos are the most used as they reduce non-radiative efficiencies by increasing the rigidity around the copper(I) center, thus avoiding the well-known pseudo-Jahn-Teller distortion in the electronic excited state.[6] Phosphines with saturated[17,18] or conjugated bridges[17,19] between the phosphorus atoms and those incorporating halides[20] or heterocyclics[21,22] into phosphines were also used to modulate the radiative and non-radiative ratio for such $[Cu(NN)(PP)]^+$ complexes. In particular, those phosphine ligands containing heteroatoms seems to enhance the photophysical properties of copper(I) complexes (See Table S1). However, the specific role of phosphines is not well known, especially when it comes to heteroatoms bonded directly to the phosphorus atom as in the aminophosphines ligands and what is their influence on the photophysical properties, calling for new phosphines and thereby establish a more comprehensive molecular design principles for copper(I)-diphosphine materials.

We report the synthesis and characterization of three luminescent Cu(I) complexes with 1,10-phenanthroline, POP,

[a] J. Toigo, G. Farias, Prof. Dr. A. J. Bortoluzzi, Prof. Dr. B. de Souza
Chemistry Department, Universidade Federal de Santa Catarina,
88040-900 Florianópolis, SC, Brazil
E-mail: bernadsz@gmail.com
[b] Dr. C. A. M. Salla, Prof. Dr. I. H. Bechtold
Physics Department, Universidade Federal de Santa Catarina,
88040-900 Florianópolis, SC, Brazil
E-mail: ivan.bechtold@ufsc.br
[c] Dr. L. G. T. A. Duarte, Prof. Dr. T. D. Zambon Atvars
Chemistry Department, Universidade Estadual de Campinas,
13083-970, Campinas, SP, Brazil

Supporting information for this article is available on the WWW under https://doi.org/10.1002/ejic.202100454

Part of the "Inorganic Chemistry in Latin America" Special Collection.

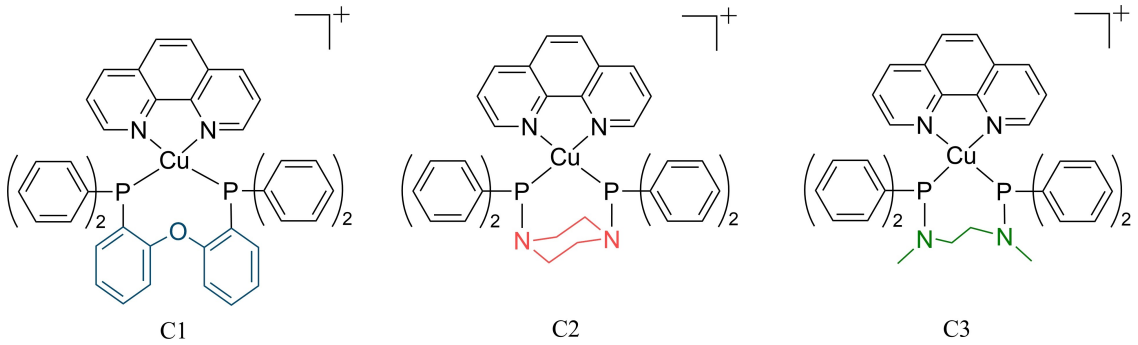

Scheme 1. Cu(I) complexes synthesized and investigated in this study.

and aminophosphine-derived ligands containing the piperazine and *N*,*N*′-dimethylethylenediamine moieties (Scheme 1). These aminophosphine ligands were chosen as they are structurally similar to others phosphines that were already studied in luminescent copper(I) complexes (2 and 3 in Table S1).[10,17] Thermal and electrochemical properties were evaluated, and aminophosphines ligands improved the thermal stability of copper(I) complexes. A detailed photophysical study was carried out, including a temperature dependence, and all complexes exhibited TADF and phosphorescence decay mechanisms. Complexes containing aminophosphine ligands showed a faster TADF decay pathway and a lower decay time than Cu(I)-POP complex. The experimental spectroscopic data have been further rationalized by means of detailed quantum-chemical calculations.

Results and Discussion

Synthesis and Structural Characterization

The Cu(I) complexes were synthesized by stirring under reflux $[Cu(CH_3CN)_4]BF_4$ in dichloromethane with the phosphine ligand for 30 minutes, then the 1,10-phenanthroline ligand was added to the mixture and kept under reflux for 1 h (see Scheme S1), as earlier reported for **C1**.[13] Complexes were obtained with excellent yields $>66\%$ and good stabilities in air under ambient conditions at least for several months without oxidizing.

Single crystals were grown from dichloromethane/ethanol (50/50 v/v) solutions by slow solvent evaporation for **C3**, and its molecular structure was determined by single-crystal X-ray diffraction studies (Figure 1). Single crystal of compound **C2**, suited for X-ray structure determination, could not be grown. X-ray diffraction analyses revealed that the copper(I) center in **C3** has a distorted tetrahedral geometry, observed by the deviation from the tetrahedral angle around the Cu(I) center, where the dihedral angle between N–Cu–N and P–Cu–P planes is 87.6°, while for **C1** it is 86.4°.[13] The Cu–P and Cu–N bond lengths and the angles around the Cu(I) atom for **C3** and those already reported to **C1** are shown in Table 1.

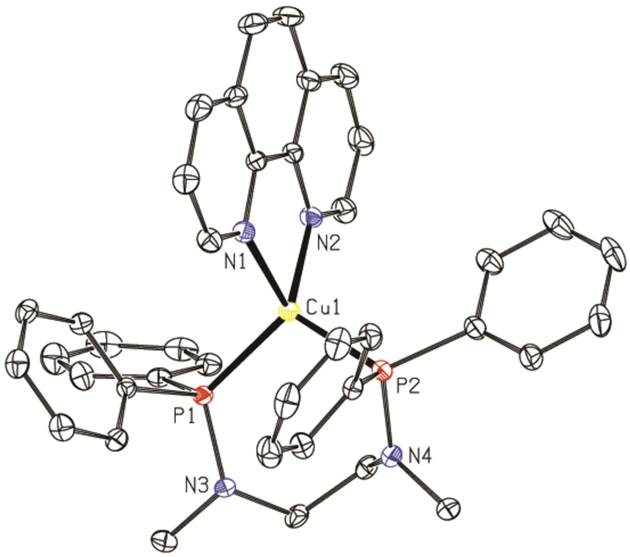

Figure 1. ORTEP plot (thermal ellipsoid with 40% probability) of the molecular structure of cation complex **C3**. Hydrogens atoms and solvent molecules are omitted for clarity.

Table 1. Selected bond lengths and angles (Å) for **C1** and **C3**.

	C1[13]	**C3**
Cu–P1	2.231	2.2233(5)
Cu–P2	2.261	2.2320(5)
Cu–N1	2.063	2.0751(14)
Cu–N2	2.071	2.0500(14)
Cu–O	3.205	–
P1–Cu–P2	108.12	109.06(18)
P1–Cu–N1	110.81	108.49(4)
P2–Cu–N2	109.08	120.41(4)
N1–Cu–N2	80.8	81.38(6)

Thermogravimetric Analysis and Cyclic Voltammetry Studies

Thermogravimetric analysis revealed that all complexes are stable until 200 °C, with the exception of **C1**, which presented an initial decomposition temperature ($T_{initial}$) close to 128 °C (Figure S4). Such thermal stability indicates that all the complexes can undergo thermal treatments until at least 100 °C.

Cyclic voltammetry in dichloromethane showed an anodic process for all the complexes (Figure S5), which is attributed to the oxidation of the copper center. The HOMO levels were estimated from the oxidation potentials (Table 2), whereas the values of LUMO energies were obtained from the optical bandgap since no cathodic process was observed in the evaluated range.[23] The complexes containing aminophosphines showed a lower potential and high HOMO energy compared with the analogous with the POP ligand, in agreement with the observed decrease of Cu–P bond lengths for **C3** in X-ray diffraction thus increasing the electronic density over the copper atom. Moreover, the HOMO and LUMO energies are in accordance with a calculated trend from DFT where the contribution of the copper atom on these orbitals was confirmed (see the theoretical modeling section). Therefore, changing POP for the aminophosphines, significantly increases the thermal stability of **C2** and **C3**, along with the oxidation potential, and consequently, the HOMO energy is only slightly shifted, which could be beneficial to OLEDs fabrication.

Photophysical Properties and detailed TADF mechanism

The UV-Vis absorption spectra were performed in both dichloromethane solution and with the complexes dispersed at 10 wt% in a PMMA matrix (Figure 2). In dichloromethane solution, the absorption spectra of **C1-C3** are very similar, showing an intense absorption band around 270 nm which is assigned as $\pi\rightarrow\pi^*$ transitions within the phosphine ligands. For these complexes, a shoulder close to 330 nm is observed and assigned to $\pi\rightarrow\pi^*$ transitions within the diimine ligand. At low energy, close to 400 nm a broad absorption band is observed, which is attributed to a metal-to-ligand charge-transfer (MLCT) transition as suggested by DFT calculations (see section 2.4).[6,7,9,12,24] The absorption spectra of the complexes dispersed in PMMA were found to be very similar to the solution (Figure S6). By exciting the complexes dispersed in PMMA at the lower energy band, a broad and unstructured line shape emission spectra was observed (Figure 2), which agrees with the MLCT nature of the emitting state (see section 2.4).

Records of the emission as a function of temperature (77 to 298 K) were carried out in solid-state, in powder form. In general, the solid-state is not suitable for detailed decay studies due to deactivation mechanisms, such as TTA and energy transfer processes. Nevertheless, copper complexes exhibit a self-trapping mechanism of the low-lying ^{1,3}MLCT states that should avoid these deactivation mechanisms.[9,25] The complexes presented intense luminescence in the yellow-orange spectral range under UV excitation (maximum absorption of the lower energy band), with emission maxima between 537 and 617 nm at 298 K and between 557 and 647 nm at 77 K (Figure S7). The emission spectra are broad and unstructured even at 77 K, which correlates with the assigned MLCT state. The blue shift from 77 to 298 K is an indication of thermal activation of the energetically higher-lying S_1 state (TADF mechanism, see below). The photoluminescence quantum yield (Φ_{PL}) is 11.8% for **C1**, 17.7% for **C2**, and 4.6% for **C3** at 298 K, and by cooling to 77 K it increases to 82.0% for **C1** and to 23.0% for **C2** and decreases to 3.2% for **C3**. The emission lifetime decay (τ) was more than one order of magnitude faster at 298 K, in μs time scale, showing a sigmoidal profile (Figure 3). Furthermore, the radiative decay rate k_r ($k_r = \Phi_{PL}/\tau$) increases at 298 K (see Table 3). The k_r changes combined with the blue shift by increasing temperature are attributed to a higher-lying energy

Table 2. Electrochemical and thermal properties of **C1**–**C3** complexes.

Complex	E_{ox} [a] [V]	E_{HOMO} [V][b]	E_{LUMO} [V][c]	Optical *Bandgap* [eV][d]	$T_{initial}$ [°C]
C1	0.84	−5.94	−3.09	2.85	128
C2	0.72	−5.82	−2.94	2.88	236
C3	0.76	−5.86	−3.23	2.63	200

[a] Determined from peak potentials; [b] Calculated from $E_{HOMO} = -(5.1 + E_{ox})$[23]; [c] Calculated from the onset of the absorption spectra in solution; [d] Obtained from the sum of the LUMO energy and optical bandgap.

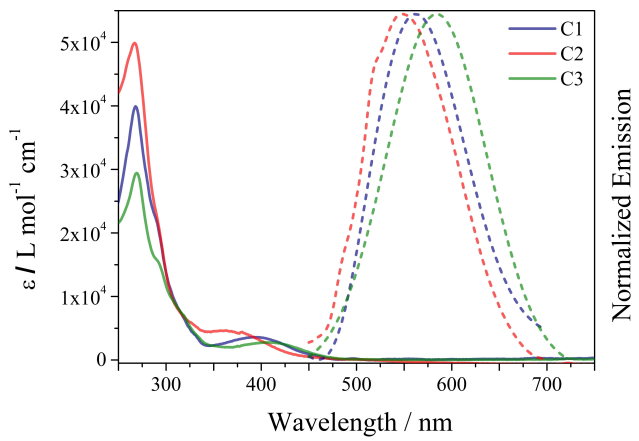

Figure 2. Optical absorption in dichloromethane solution 1.0×10^{-5} mol L^{-1} (solid lines) and emission spectra at 10 wt% in PMMA (dashed lines) of the Cu(I) complexes. Emission spectra were obtained with excitation at maximum absorption of the lower energy band.

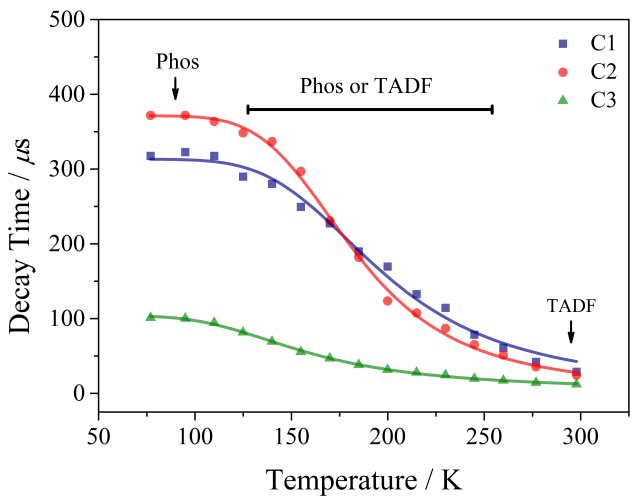

Figure 3. Temperature dependence of the emission decay time of **C1-C3** powder and fit according to Eq. (1).

Table 3. Summary of photophysical properties at 298 and 77 K of the Cu(I) complexes in powder.

		C1	C2	C3
298 K	λ_{em} [nm]	537	573	617
	τ [μs]	28.87	24.28	12.10
	Φ [%]	11.8	17.7	4.6
	k_r[a] [s^{-1}]	4.09×10^3	7.29×10^3	3.80×10^3
	k_{nr}[b] [s^{-1}]	3.05×10^4	3.39×10^4	7.88×10^4
77 K	λ_{em} [nm]	557	587	647
	τ [μs]	317.46	371.74	101.01
	Φ [%]	82.0	23.0	3.2
	k_r[a] [s^{-1}]	2.58×10^3	6.19×10^2	3.17×10^2
	k_{nr}[b] [s^{-1}]	5.67×10^2	2.07×10^3	9.58×10^3
	k_{S1}[c] [s^{-1}]	2.68×10^6	5.92×10^6	2.34×10^6
	k_{T1}[c] [s^{-1}]	3.19×10^3	2.69×10^3	9.65×10^3
	ΔE_{ST}[c] [cm^{-1}]	781	844	495
	k_{TADF}[d] [s^{-1}]	3.14×10^4	3.85×10^4	7.30×10^4

[a] $k_r = \frac{\Phi}{\tau}$; [b] $k_{nr} = \frac{(1-\Phi)}{\tau}$; [c] Values were obtained by the fit to the equation (1); [d] $k_{TADF} = \frac{1}{\tau\,(298\,K)} - k_{T1}$.

emitting state. In this case, the S_1 (or the ^{1}MLCT) that carries a high radiative rate being thermally populated by a lower energy state, the T_1 (or the ^{3}MLCT), hence demonstrating the occurrence of TADF. Due to this thermal equilibrium between the S_1 and T_1, the emission lifetime decay can be expressed by a Boltzmann-type equation:[7–10,26,27]

$$\tau(T) = \frac{3 + \exp\left(-\frac{\Delta E_{ST}}{k_B T}\right)}{\frac{3}{\tau_{T_1}} + \frac{1}{\tau_{S_1}} \times \exp\left(-\frac{\Delta E_{S_1-T_1}}{k_B T}\right)} \quad (1)$$

wherein k_B denotes the Boltzmann constant. $\tau(T_1)$ and $\tau(S_1)$ represent the phosphorescence (Phos) and prompt fluorescence (PF) decay times without thermal activation. $\Delta E(S_1–T_1)$ is the energy separation between these two states.

Fitting of Eq. 1 to the experimental data of emission decay time of compound **C1** (Figure 3, blue line in the lifetime decay profiles) led to a good fitting of the data and allows the determination of the individual emission decays and energy gap between the S_1 and T_1 states. An energy separation of $\Delta E(S_1–T_1) = 781\ cm^{-1}$ and lifetimes of $\tau(S_1) = 374$ ns and $\tau(T_1) = 313\ \mu s$ was obtained. The obtained $\tau(S_1) = 374$ ns for PF is related here to probability of the $S_1 \rightarrow S_0$ transition, as the ISC is faster than nanoseconds frame and effectively quenches the PF. Using the obtained Phos rate of $k(T_1) = (313\ \mu s)^{-1}$, the TADF rate can be determined[7,9] by $k_{TADF} = k_{combined} - k_{T1}$, where k-(combined) $= \tau^{-1}$ (298 K) $= (28.87\ \mu s)^{-1}$. The TADF-only decay time amounts to about 32 μs. With the additional decay channel via the triplet state the overall decay time by ~39 %.[25] Figure 4a summarizes the relevant emission processes for **C1** in a simplified Jablonski diagram.

Analogous studies were performed for **C2** and **C3** and the same temperature dependence in emission characteristic of a

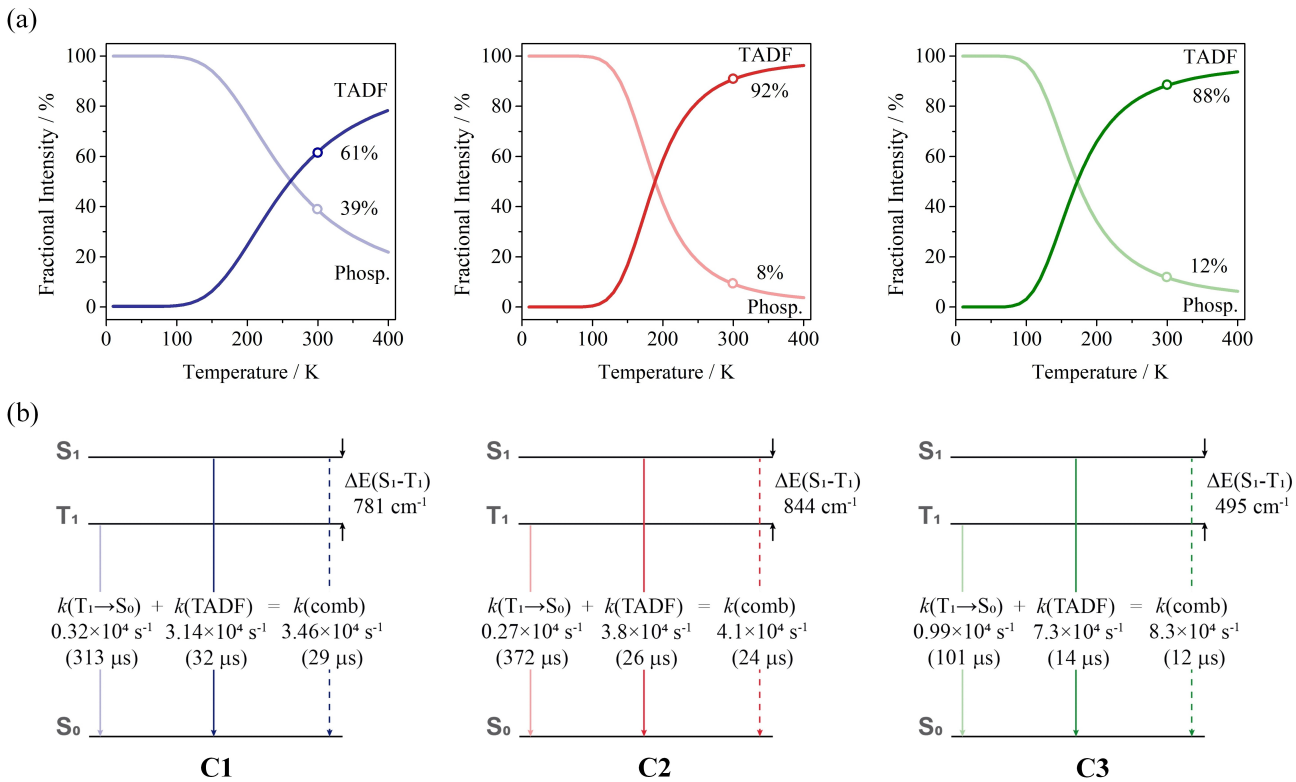

Figure 4. (a) Fractional emission intensities (simulation results) stemming from TADF and direct Phos as a function of temperature, respectively, calculated on the basis of the experimental data from Figure 3.[25] The points characterize the properties of compounds at room temperature. (b) Schematic energy level diagram with state-related decay rates (times) of **C1**–**C3** in powder.

TADF mechanism was observed. The energy separation of $\Delta E(S_1–T_1)$ obtained for **C2** and **C3** was 844 and 495 cm^{-1}, respectively. This distinct $\Delta E(S_1–T_1)$ can be explained by the spatial separation between HOMO and LUMO, as discussed below. The radiative rates of triplet T_1 states vary from 3.19×10^3 (**C1**) to 2.69×10^3 (**C2**) to 9.65×10^3 (**C3**). It suggests that the SOC efficiency decreases for **C2** and increases for **C3**, which is confirmed by the calculated SOC matrix elements (see below). Interestingly, for the complex **C3**, even with a higher k_{T1} the quantum yield decreases at low temperature for this complex. It is attributed to the lower triplet energy, which should increase the overlap of the triplet and ground-state potential energy surfaces and thus enhance the non-radiative decay at low temperatures. In contrast, at room temperature, the TADF pathway competes and thus increases the quantum yield. The obtained $k(S_1)$ was higher for **C2** and lower for **C3** compared to **C1**, in agreement with the high molar absorptivity observed in the UV-Vis data, indicating a higher oscillator strength for the $S_1\rightarrow S_0$ transition in the order **C2** > **C1** > **C3**. Finally, the k_{TADF} slightly increases from **C1** to **C2** and increases by a factor of ~2.4 for **C3**. For **C2**, this is mostly attributed to the higher oscillator strength for the $S_1\rightarrow S_0$ transition, despite the $\Delta E(S_1–T_1)$ increase for this complex. On other hand, for **C3** the changes occur due to the lower $\Delta E(S_1–T_1)$, which significantly favors the TADF decay pathway. For both **C2** and **C3**, the TADF pathway contribution is higher than for **C1**. The additional decay channel via the triplet state to the overall decay time contributes by ~8% for **C2** and ~12% for **C3**.

Theoretical Modeling of the Electronic Structure and Photophysical Interpretations

DFT calculations were carried out at the PBE0/def2-TZVP(-f) level of theory to support our experimental results. The ground state geometries (Figure S8) were obtained, and for **C1** and **C3**, the predicted geometries were in good agreement with the X-ray structure, where the maximum average errors found for bond lengths and bond angles were 1%, and 3%, respectively.

For these complexes, the HOMO has significant contributions from 3*d* orbitals centered in the copper(I) atom, as well as from the coordinated phosphorus atoms, where the complexes containing the aminophosphines have a greater contribution of phosphorus and nitrogen orbitals of the aminophosphine. On the other hand, the LUMO is mainly distributed over the diamine (Figure 5). Thus, the lower energy excited states are expected to be MLCT-like. In fact, TD-DFT calculations showed that the low-lying S_1 and T_1 states are more than 88% HOMO→LUMO transitions in S_1 and mixed HOMO→LUMO and HOMO→LUMO-1 (both MLCT) for T_1 (Table S5–S6), being assigned as ^{1}MLCT and ^{3}MLCT, respectively.

The HOMO orbital centered at copper-aminophosphine moiety maximize the HOMO and LUMO overlap for **C2**, while it is minimized for **C3** by decreasing or increasing the spatial separation of these orbitals, respectively (Figure S9). The HOMO and LUMO overlap directly impacts the $\Delta E(S_1–T_1)$,[24] as observed from the spectroscopic studies, and agrees well with the calculated $\Delta E(S_1–T_1)$ using the vertical energy difference for such states (Table 4). The computed energy separation shows higher values than the experimental ones due to a known issue in DFT for such charge transfer states.[28] The spatial separation of HOMO and LUMO also impacts the oscillator strength *f* of the $S_0\rightarrow S_1$ transition (^{1}MLCT) for complexes with aminophosphine ligands. The calculated *f* follows the same trend observed at the UV-Vis experiments for the MLCT transition and the comparison between the calculated and experimental absorption spectra is shown in Figure S10.

The SOC matrix elements between the first 10 singlet and triplet states were calculated to evaluate their influences on the Phos and the TADF decay pathways for **C1-C3** on top of S_0 geometries.[29] The SOC matrix elements, between the first four singlets and the first three triplet states, which should have an appreciable contribution to the Phos and the TADF mechanism in these complexes, are shown in Table 4. As one can see, the SOC between S_1 and T_1, both mainly involving the MLCT transitions with the same *d* orbital, decrease for complexes with the aminophosphines, which is related to the very similar configuration for both singlet and triplet states. Also, as the SOC matrix elements have a distance dependence, it was observed that the aminophosphine ligands have a HOMO more spread through the phosphine and less present over the copper atom. Because of the close similarity in both energy and size of these the atomic orbitals of P and Cu, such results were expected. Also, the fact that the copper atom contributes

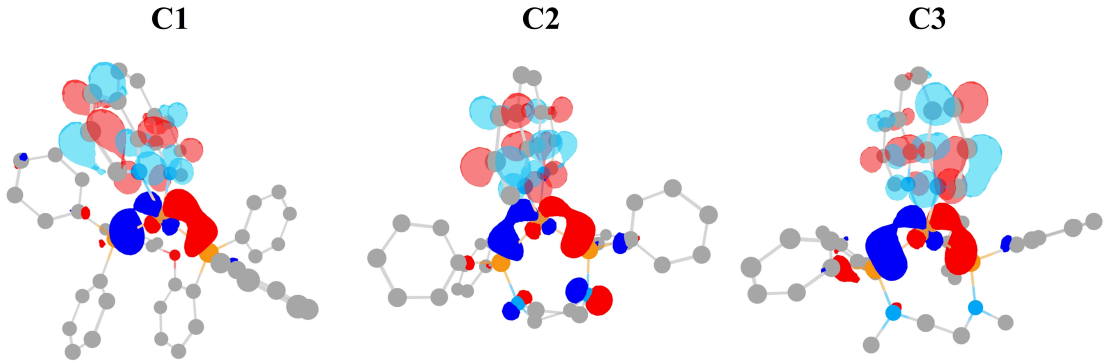

Figure 5. Frontier molecular orbitals of complexes **C1**–**C3** calculated using PBE0/def2-TZVP(-f). The LUMO is shown as the isosurface with transparency.

Table 4. Data of SOC-TD-DFT (in cm^{-1}) and vertical energy difference for **C1**–**C3**.

	C1	C2	C3
$\langle T_1\|H_{SO}\|S_0\rangle$ [a]	36.79	16.04	21.90
$\langle T_1\|H_{SO}\|S_1\rangle$ [a]	27.65	12.43	18.30
$\langle T_1\|H_{SO}\|S_2\rangle$ [a]	6.32	3.22	6.84
$\langle T_1\|H_{SO}\|S_3\rangle$ [a]	119.62	102.84	157.40
$\langle T_1\|H_{SO}\|S_4\rangle$ [a]	128.53	13.33	151.83
$\langle T_2\|H_{SO}\|S_0\rangle$ [a]	12.33	11.52	15.84
$\langle T_2\|H_{SO}\|S_1\rangle$ [a]	21.16	10.61	20.84
$\langle T_2\|H_{SO}\|S_2\rangle$ [a]	13.55	4.48	10.16
$\langle T_2\|H_{SO}\|S_3\rangle$ [a]	34.32	10.70	20.08
$\langle T_2\|H_{SO}\|S_4\rangle$ [a]	87.76	82.85	41.72
$\langle T_3\|H_{SO}\|S_0\rangle$ [a]	74.12	62.86	78.47
$\langle T_3\|H_{SO}\|S_1\rangle$ [a]	99.61	89.05	131.61
$\langle T_3\|H_{SO}\|S_2\rangle$ [a]	19.80	8.97	17.79
$\langle T_3\|H_{SO}\|S_3\rangle$ [a]	7.63	2.27	5.84
$\langle T_3\|H_{SO}\|S_4\rangle$ [a]	54.22	2.46	123.45
$\Sigma \langle T_j\|\hat{H}_{SO}\|S_i\rangle$	684.53	352.82	899.95
S_1 [b] [eV]	2.79	2.40	2.68
T_1 [b] [eV]	2.42	1.96	2.27
$\Delta E(S_1–T_1)$ [b] [eV]	0.37	0.44	0.41
S_1 [c] [eV]	2.71	2.58	2.48
T_1 [c] [eV]	2.63	2.45	2.42
$\Delta E(S_1–T_1)$ [d] [eV]	0.10	0.11	0.06

[a] $\sqrt{\langle (S_i\,|\,H_{SO}\,|\,T_{j\,(MS=0,\pm1)})^2\rangle}$ in the S_0 geometry; [b] Vertical energy difference from SOC-TD-DFT; [c] Experimental data obtained from the onset of the emission spectra at room temperature and 77 K; [d] $\Delta E(S_1–T_1)$ obtained from the Boltzmann-type fitting.

strongly to the molecular orbital, and that it has a larger SOC constant, makes the SOC matrix elements increase. However, as mentioned, the TADF pathway relies both in the energy gap between the S_1 and T_1 states and the oscillator strength of the $S_0 \rightarrow S_1$ transition, and even with small SOC matrix elements between the S_1 and T_1 states for **C2** and **C3**, these complexes showed a faster TADF decay pathway. By adding these SOC matrix elements, one can more accurately reflect the phosphorescence decay pathway.[26] In Table 4, the sum of SOC matrix elements for these complexes follows the order **C3** > **C1** > **C2**, which is the same order of the triplet radiative constant obtained experimentally. However, the non-radiative pathway from the triplet state also increases for **C2** and **C3** as the triplet energy decreases for these complexes (Table 4).

It is possible to conclude that even structurally similar, the aminophosphine ligands significantly change the photophysical properties, for complexes **C2** and **C3**. For these complexes, the introduction of aminophosphine ligands resulted in a faster TADF decay pathway, mainly due to the degree of the HOMO and LUMO overlap. For **C2** the Phos decay pathway was slower than **C1** but compensated by the higher contribution of the faster TADF to the overall decay. For **C3**, the combined lower $\Delta E(S_1–T_1)$, and high SOC suited to enhance both the TADF and phosphorescence decay pathways resulted in an even faster overall decay. For both complexes with aminophosphines, the non-radiative pathway was also enhanced thus impacting the emission quantum yield, especially for **C3**. Besides, the aminophosphines ligands showed significant decrease of the overall lifetime, which can be explored further in more efficient materials.

Conclusion

We have systematically investigated the electronic and structural properties of three luminescent $[Cu(NN)(PP)]^+$ complexes by using three different phosphine ligands. The aminophosphines increased the thermal stability of **C2** and **C3**, while the oxidation potential is slightly shifted. All compounds exhibited combined TADF and phosphorescence decays as determined by time-resolved and temperature-dependent emission spectroscopy. The complexes containing aminophosphines ligands showed a reduction of the overall lifetime, as a result of a higher contribution of the TADF decay pathway. This was achieved by decreasing the $\Delta E(S_1–T_1)$ energy gap for **C3** and by the increasing the oscillator strength of the $S_1 \rightarrow S_0$ transition in **C2. C3** also showed a faster phosphorescence decay pathway due to the higher SOC between the low-lying states as computed by SOC-TD-DFT. Although the non-radiative pathway was enhanced in these complexes, the higher radiative pathway and the shorter lifetime could be highly advantageous for application in OLED as emitter. These results contribute to a deeper insight into modulating photophysical properties by ligands, leading to more efficient devices based on copper(I) complexes.

Experimental section

General procedures

All starting materials were purchased from commercial suppliers and were used without further purification, while solvents were dried with Na/NaH and storage over drying agents. Thin layer chromatography (TLC) was carried out on silica gel. The measurements of carbon, hydrogen and nitrogen percentages for synthesized complexes were performed on a C, H, N – Perkin-Elmer 2400 elemental analyzer. The spectra in the infrared region were obtained in a Perkin Elmer Spectrum 100 spectrophotometer, in the region of 4000 to 450 cm^{-1}. The method of attenuated total reflectance (ATR) was used to analyze all samples.

The X-ray diffraction analysis was performed on a Bruker APEX II DUO diffractometer using radiation generated by a molybdenum tube (MoKα $\lambda = 0.71073$ Å) and graphite monochromator. During the analysis the sample was sustained at 200 K. The crystalline structure was solved by direct methods and refined by the least squares method with complete matrix, using the programs SIR97[30] and SHELXL-97,[31] respectively. The graphical representations of the molecular structures were generated using the program PLATON.[32] Selected crystallographic data are presented in SI file and full crystallographic tables (including structure factors) have been deposited.

Synthesis and characterization

1,4-bis(diphenylphosphino)piperazine (PNNP) N,N,N′,N′-tetramethylethylenediamine (1.5 mL, 10.0 mmol) was added dropwise to a two-necked flask filled with argon and charged with 4,2 mL of a 2.64 N solution of butyllithium (10.0 mmol) at room temperature. A solution of 0,43 g (5 mmol) of piperazine in 5 ml of dry tetrahydrofuran was slowly added. The mixture was stirred for 6 h. A solution of 1.8 mL (10.0 mmol) of chlorodiphenylphosphine in 5 ml of ethyl ether was added dropwise to the reaction mixture. The

mixture was stirred for 16 h at 25 °C, 10 ml of distilled water and 10 ml of dichloromethane were added, the organic phase was separated, dried over sodium sulfate, and the solvent was removed under reduced pressure. The residue was dissolved in 10 mL, the solution was cooled to 10 °C and colorless precipitate was obtained. Yield 32 %, mp 133–135; ^{1}H NMR (200 MHz, $CDCl_3$): δ (ppm) 7.36 (m, 20H), 2.88 (m, 8H); ^{31}P NMR (200 MHz, $CDCl_3$): δ (ppm) 62.96 (s).

N1,N2-bis(diphenylphosphino)-N1,N2-dimethylethane-1,2-diamine (Me-PNNP) The ligand was prepared using the similar procedure described for PNNP. Yield 22 %, mp 114–116; ^{1}H NMR (200 MHz, $CDCl_3$): δ (ppm): 7.35 (m, 20H), 3.21–3.16 (dd, J = 3.85 e 6.48 Hz, 4H), 2.51–2.48 (d, J = 5.81 Hz, 6H); ^{31}P NMR (200 MHz, $CDCl_3$): δ (ppm) 65.38 (s).

[Cu(Phen)(POP)]BF_4 (**C1**). The synthesis of the cationic complexes was performed by dissolving 105 mg of POP (0.2 mmol) in dry dichloromethane (20 mL) under argon. Tetrakis(acetonitrile) copper(I) tetrafluoroborate (63 mg, 0.2 mmol) was added to this solution, and the reaction mixture was refluxed for 30 min. Then Phen (40 mg, 0.2 mmol) was added. The mixture was refluxed for another half hour. Possible residues were filtered off and the solvent was removed under vacuum evaporation. The crude product was further purified by recrystallization from the mixed solvent of dichloromethane/ethanol (50 : 50). Yield: 87 %; IR (cm^{-1}): ν (C–H_{ar}) 3058, ν (C=N e C=C) 1433, ν (C–O) 1210, ν (B–F) 1041; δ (C–H_{ar}) 846–693; $C_{52.5}H_{45}BClCuF_4N_2O_2P_2$: calcd. C 64.52, H 4.77, N 2.95; found C 64.76, H 4.64, N 2.89.

[Cu(Phen)(PNNP)]BF_4 (**C2**). **C2** was synthesized by a method similar to that of **C1**, except that POP was replaced by PNNP. Yield: 82 %; IR (cm^{-1}): ν (C–H_{ar}) 3051, ν (C–H_{al}) 2910, ν (C=N e C=C) 1482–1256, ν (B–F) 1080; δ (C–H_{ar}) 957–621; $C_{40}H_{36}BCuF_4N_4P_2$: calcd. C 61.20, H 4.62, N 7.14; found C 61.50, H 4.74, N 6.89.

[Cu(Phen)(Me-PNNP)]BF_4 (**C3**). **C3** was synthesized by a method similar to that of **C1**, except that POP was replaced by Me-PNNP. Yield: 66 %; IR (cm^{-1}): ν (C–H_{ar}) 3045, ν (C–H_{al}) 2911–2808, ν (C=N e C=C) 1482–1142; ν (B–F) 1044; δ (C–H_{ar}) 1436–642; $C_{40}H_{38}BCuF_4N_4P_2$: calcd. C 61.04, H 4.87, N 7.12; found C 61.40, H 4.80, N 7.15.

Thermogravimetric Analysis and Cyclic Voltammetry Studies

The thermogravimetric analysis was performed using a Shimadzu, model TGA-50. For each experiment, approximately 2 mg of sample were weighed in a platinum crucible, with a nitrogen flow of 100 mL min^{-1} and a heating ramp of 10 °C min^{-1} in a temperature range of 30–900 °C.

The redox behavior of the complexes was investigated by square wave voltammetry in a potentiostat-galvanostat BAS (Bioanalytical Systems, Inc.) model Epsilon. A concentration of 2×10^{-5} mol L^{-1} in dichloromethane solution was used under nitrogen atmosphere. Tetrabutylammonium hexafluorophosphate (0.1 mol L^{-1}) was used as support electrolyte and the electrochemical cell was composed of three electrodes: work – gold; auxiliary – platinum wire; reference – Ag/Ag^+. For correction of the reference electrode the ferrocene ($E_{1/2}$ *vs* NHE = 398 mV) was used.

Spectroscopic Measurements

The electronic spectra in the ultraviolet, visible and near infrared regions were obtained for all the complexes in the range of 250–800 nm in a Perkin-Elmer spectrophotometer model Lambda-750. The values of ε are given in L mol^{-1} cm^{-1}. Absolute quantum yields (Φ) at ambient temperature and at 77 K were carried out with a Hamamatsu Photonics Absolute Quantum Yield Measurement System model c9920-02G which is based on the integrating sphere method.

The time-resolved emission spectra were obtained by use of a Horiba FL3-22-iHR320 spectrofluorometer by the Time-Correlated Single Photon Count (TCSPC) technique. For excitation, a flash 150 W xenon lamp was used. The detection system consists of a monochromator and a multi-channel base photomultiplier (Hamamatsu R3809 U-50). The temperature-dependent luminescence spectra were recorded in a spectrofluorometer with the sample in a chamber of a cryostat (Linkam THMS600) operating in different temperatures, with a thermal stabilization of 15 min between measurements. The emission decay curves were fitted using exponential functions using a FAST software (provided by Edinburg). Fitting quality was evaluated by χ^2 error and to the residual distribution.

Theoretical methods

Geometry optimizations of complexes **C1-C3** were performed in a vacuum at the density functional theory (DFT) level using the PBE0[33,34] and Def2-TZVP(-f)[35,36] basis set. Grimme's dispersion correction with damping D3BJ[37,38] and the resolution of identity approximation for the Coulomb part, with the corresponding auxiliary basis, were also included. To verify that ground state is minima on the potential energy surface, analytical harmonic vibrational frequency calculations were conducted. Time-dependent density functional theory (TD-DFT)[39] was employed to obtain the first 50 singlet excited states, including the solvent correction using a continuous polarizability model method (CPCM).[40] The SOC on top of the TD-DFT results were done by using quasi-degenerate perturbation theory.[29,41] The SOC integrals used here are calculated using a mean-field approach named as RI-SOMF(1X) described elsewhere.[42] Furthermore, all the calculations were performed using Orca 4.1.2[43] and the geometric representations of the complexes were obtained using the Chemcraft program.[44]

Deposition Number 2083919 (for C**3**) contains the supplementary crystallographic data for this paper. These data are provided free of charge by the joint Cambridge Crystallographic Data Centre and Fachinformationszentrum Karlsruhe Access Structures service www.ccdc.cam.ac.uk/structures.

Acknowledgements

The authors are grateful to CNPq, CAPES, FAPESC, FAPESP (grant number 2013/16245-2), INCT-INEO and H2020-MSCA-RISE-2017 (OCTA, #778158) for financial support of this work.

Conflict of Interest

The authors declare no conflict of interest.

Keywords: Aminophosphines · Copper(I) complexes · Luminescence · TADF

[1] Z. Yang, Z. Mao, Z. Xie, Y. Zhang, S. Liu, J. Zhao, J. Xu, Z. Chi, M. P. Aldred, *Chem. Soc. Rev.* **2017**, *46*, 915–1016.
[2] C. Bizzarri, E. Spuling, D. M. Knoll, D. Volz, S. Bräse, *Coord. Chem. Rev.* **2018**, *373*, 49–82.

[3] F. Dumur, *Org. Electron.* **2015**, *21*, 27–39.
[4] Y. Liu, C. Li, Z. Ren, S. Yan, M. R. Bryce, *Nat. Rev. Mater.* **2018**, *3*, 1–20.
[5] C. Murawski, K. Leo, M. C. Gather, *Adv. Mater.* **2013**, *25*, 6801–6827.
[6] Y. Zhang, M. Schulz, M. Wächtler, M. Karnahl, B. Dietzek, *Coord. Chem. Rev.* **2018**, *356*, 127–146.
[7] H. Yersin, R. Czerwieniec, M. Z. Shafikov, A. F. Suleymanova, *ChemPhysChem* **2017**, *18*, 3508–3535.
[8] D. S. M. Ravinson, M. E. Thompson, *Mater. Horiz.* **2020**, *7*, 1210–1217.
[9] R. Czerwieniec, M. J. Leitl, H. H. H. Homeier, H. Yersin, *Coord. Chem. Rev.* **2016**, *325*, 2–28.
[10] R. Czerwieniec, H. Yersin, *Inorg. Chem.* **2015**, *54*, 4322–4327.
[11] Q. Zhang, J. Chen, X.-Y. Wu, X.-L. Chen, R. Yu, C.-Z. Lu, *Dalton Trans.* **2015**, *44*, 6706–6710.
[12] D. R. McMillin, J. R. Kirchhoff, K. V. Goodwin, *Coord. Chem. Rev.* **1985**, *64*, 83–92.
[13] K. Zhang, D. Zhang, *Spectrochim. Acta Part A* **2014**, *124*, 341–348.
[14] S.-M. Kuang, D. G. Cuttell, D. R. McMillin, P. E. Fanwick, R. A. Walton, *Inorg. Chem.* **2002**, *41*, 3313–3322
[15] D. Liang, X.-L. Chen, J.-Z. Liao, J.-Y. Hu, J.-H. Jia, C.-Z. Lu, *Inorg. Chem.* **2016**, *55*, 7467–7475.
[16] E. Mejía, S.-P. Luo, M. Karnahl, A. Friedrich, S. Tschierlei, A.-E. Surkus, H. Junge, S. Gladiali, S. Lochbrunner, M. A. Beller, *Chem. Eur. J.* **2013**, *19*, 15972–15978.
[17] E. Leoni, J. Mohanraj, M. Holler, M. Mohankumar, I. Nierengarten, F. Monti, A. Sournia-Saquet, B. Delavaux-Nicot, J.-F. Nierengarten, N. Armaroli, *Inorg. Chem.* **2018**, *57*, 15537–15549.
[18] R. Czerwieniec, K. Kowalski, H. Yersin, *Dalton Trans.* **2013**, *42*, 9826–9830.
[19] H. Yersin, M. J. Leitl, R. Czerwieniec, *Proc. SPIE* **2014**, *9183*, 91830N.
[20] S. Igawa, M. Hashimoto, I. Kawata, M. Yashima, M. Hoshino, M. Osawa, *J. Mater. Chem. C* **2013**, *1*, 542–551.
[21] X. Li, J. Zhang, Z. Zhao, X. Yu, P. Li, Y. Yao, Z. Liu, Q. Jin, Z. Bian, Z. Lu, C. Huang, *ACS Appl. Mater. Interfaces* **2019**, *11*, 3262–3270.
[22] D. M. Zink, D. Volz, T. Baumann, M. Mydlak, H. Flügge, J. Friedrichs, M. Nieger, S. Bräse, *Heteroleptic, Chem. Mater.* **2013**, *25*, 4471–4486.
[23] C. M. Cardona, W. Li, A. E. Kaifer, D. Stockdale, G. C. Bazan, *Adv. Mater.* **2011**, *23*, 2367–2371.
[24] G. Farias, C. A. M. Salla, R. S. Heying, A. J. Bortoluzzi, S. F. Curcio, T. Cazati, P. L. dos Santos, A. P. Monkman, B. de Souza, I. H. Bechtold, Reducing *J. Mater. Chem. C* **2020**, *8*, 14595–14604.
[25] H. Yersin, A. F. Rausch, R. Czerwieniec, T. Hofbeck, T. Fischer, *Coord. Chem. Rev.* **2011**, *255*, 2622–2652.
[26] T. Hofbeck, U. Monkowius, H. Yersin, *J. Am. Chem. Soc.* **2015**, *137*, 399–404.
[27] A. Schinabeck, M. J. Leitl, H. Yersin, *J. Phys. Chem. Lett.* **2018**, *9*, 2848–2856.
[28] C. A. Guido, S. Knecht, J. Kongsted, B. Mennucci, *J. Chem. Theory Comput.* **2013**, *9*, 2209–2220.
[29] B. de Souza, G. Farias, F. Neese, R. Izsák, *J. Chem. Theory Comput.* **2019**, *15*, 1896–1904.
[30] A. Altomare, M. C. Burla, M. Camalli, G. L. Cascarano, C. Giacovazzo, A. Guagliardi, A. G. G. Moliterni, G. Polidori, R. Spagna, *J. Appl. Crystallogr.* **1999**, *32*, 115–119.
[31] G. M. Sheldrick, *SHELXS-97: Program for the Solution of Crystal Structures* University of Gottingen, Alemanha, **1997**.
[32] A. L. Spek, *Acta Crystallogr. Sect. D* **2009**, *65*, 148–155.
[33] J. P. Perdew, K. Burke, M. Ernzerhof, *Phys. Rev. Lett.* **1996**, *77*, 3865–3868.
[34] J. P. Perdew, K. Burke, M. Ernzerhof, *Phys. Rev. Lett.* **1997**, *78*, 1396–1396.
[35] F. Weigend, R. Ahlrichs, *Phys. Chem. Chem. Phys.* **2005**, *7*, 3297–3305.
[36] A. Schäfer, C. Huber, R. Ahlrichs, *J. Chem. Phys.* **1994**, *100*, 5829–5835.
[37] S. Grimme, J. Antony, S. Ehrlich, H. Krieg, *J. Chem. Phys.* **2010**, *132*, 154104.
[38] S. Grimme, S. Ehrlich, L. Goerigk, *J. Comb. Chem.* **2011**, *32*, 1456–1465.
[39] T. Petrenko, S. Kossmann, F. Neese, *J. Chem. Phys.* **2011**, *134*, 054116.
[40] A. V. Marenich, C. J. Cramer, D. G. Truhlar, *J. Phys. Chem. B* **2009**, *113*, 6378–6396.
[41] B. de Souza, F. Neese, R. Izsák, *J. Chem. Phys.* **2018**, *148*, 034104.
[42] F. Neese, *J. Chem. Phys.* **2005**, *122*, 034107.
[43] F. Neese, *Wiley Interdiscip. Rev.: Comput. Mol. Sci.* **2018**, *8*, e1327.
[44] http://www.chemcraftprog.com.

Manuscript received: May 24, 2021
Revised manuscript received: July 8, 2021
Accepted manuscript online: July 11, 2021

FULL PAPERS

We investigated three copper(I) complexes, two with aminophosphine ligands. These aminophosphine ligands are able to speed up the TADF pathway in copper complexes, one by decreasing the energy gap between S_1 and T_1 states and the other by increasing the allowedness of the singlet pathway. The presented table of context shows one of these complexes and indicates their faster TADF.